Excited states of two-dimensional solitons supported by spin-orbit coupling and field-induced dipole-dipole repulsion

Chunqing Huang,[1] Yuebo Ye,[1] Shimei Liu,[1] Hexiang He,[1] Wei Pang,[2] Boris A. Malomed,[3,4,1] and Yongyao Li[1,*]

[1]*School of Physics and Optoelectronic Engineering, Foshan University, Foshan 528000, China*

[2]*Department of Experiment Teaching, Guangdong University of Technology, Guangzhou 510006, China*

[3]*Department of Physical Electronics, School of Electrical Engineering, Faculty of Engineering, and the Center for Light-Matter Interaction, Tel Aviv University, Tel Aviv 69978, Israel*

[4]*ITMO University, St. Petersburg 197101, Russia*

(Received 19 July 2017; published 30 January 2018)

It was recently found that excited states of semivortex and mixed-mode solitons are unstable in spin-orbit-coupled Bose-Einstein condensates (BECs) with contact interactions. We demonstrate a possibility to stabilize such excited states in a setting based on repulsive dipole-dipole interactions induced by a polarizing field, oriented perpendicular to the plane in which the dipolar BEC is trapped. The strength of the field is assumed to grow in the radial direction $\sim r^4$. Excited states of semivortex solitons have vorticities S and $S+1$ in their two components, each being an eigenstate of the angular momentum. They are fully stable up to $S=5$. The excited state of mixed-mode solitons feature interweaving necklace structures with opposite fractional values of the angular momentum in the two components. They are stable if they are built of dominant angular harmonics $\pm S$, with $S \leqslant 4$. The characteristics and stability of these two types of previously unknown higher-order solitons are systematically analyzed. Their characteristic size is $\sim 10\,\mu$m, with the number of atoms $\lesssim 10^5$.

DOI: 10.1103/PhysRevA.97.013636

I. INTRODUCTION AND MODEL

Stabilizing bright solitary waves and vortices in the two- and three-dimensional (2D and 3D) free space with cubic nonlinearity remains a problem of great interest in nonlinear optics and studies of Bose-Einstein condensates (BECs), as well as in other areas [1,2]. A well-known challenging problem is that the ubiquitous cubic local attractive nonlinearity makes multidimensional solitons unstable against collapse. Diverse methods have been proposed to suppress this instability. In particular, in nonlinear optics stable 2D optical solitons have been predicted and created in media with saturable [3], quadratic [4], cubic-quintic [5], and nonlocal nonlinearities [6–8], which do not cause collapse.

It has been predicted too that long-range dipole-dipole interactions can create 2D matter-wave solitons in BECs with permanent atomic and molecular magnetic or electric dipole moments [9–14]. Because dipole-dipole interactions can be tuned to be isotropic or anisotropic by choosing the orientation of the external polarizing field with respect to the system's plane, this makes the dipolar BECs appropriate media for simulating 2D and 3D solitons and solitary vortices.

In addition to the stabilization induced by dipole-dipole interactions, it has also been predicted that 2D and 3D solitons can be stabilized in spinor (two-component) BECs with the help of Rashba-type spin-orbit (SO) coupling [15–23] . Similar to dipole-dipole interactions, SO coupling in BECs [24–26] provides broad tunability for the formation of solitons [27–33] . To date, two types of stable multidimensional solitons, *viz.*, semivortices (SVs, also called half-vortices [34]) and mixed-mode (MM) states, have been predicted in SO-coupled BECs. More complex self-trapped modes, which may be considered as excited states of SVs and MMs, produced by adding the same vorticity to both components of the binary soliton, are also supported by the Rashba SO coupling. Excited states of SVs and MMs exhibit complex patterns, which may be of considerable interest to the soliton physics, if they can be made stable. In reality, all the previously studied excited states were found to be unstable under the action of local and nonlocal attractive nonlinearities [16,22], quickly or gradually decaying back to their ground-state counterparts, or completely losing the soliton structure.

The objective of this work is to predict stable excited states and study their properties in SO-coupled BECs, using a nonlocal *repulsive* nonlinearity. Recently, we found that BECs with repulsive dipole-dipole interactions can support stable 2D gap solitons with large values of embedded vorticity, shaped as vortex rings [35]. This finding suggests that repulsive dipole-dipole interactions may be an appropriate means for stabilizing other types of 2D solitons, including excited states in SO-coupled BECs.

Of course, repulsive nonlinearity cannot create bright soliton in free space (without the help of a trapping potential; in models of the nonlinear Dirac or Weyl type, which do not contain the usual kinetic-energy terms, repulsive dipole-dipole interactions can support bright gap soliton in the free space for the SO-coupled BEC, under the action of the Zeeman splitting [36]). On the other hand, it was reported that bright fundamental and vortex 2D solitons can be supported by spatially patterned repulsive dipole-dipole interactions, induced by a nonuniform polarizing field, the strength of which grows from

*yongyaoli@gmail.com

 ©2018 American Physical Society

the center to periphery, as a function of distance r, at any rate faster than r^3 [37,38]. Similar settings, using spatially varying contact (local) self-repulsion, the strength of which grows, in the space of dimension D, faster than r^D [39–43], have been reported to support robust families of complex modes, such as hopfions [44], which carry two independent topological charges.

We aim to predict stable excited states of SVs and MM in a similar 2D system, using the repulsive interaction whose strength grows from the center to the periphery. While this possibility can be realized with both local (contact) and nonlocal (dipole-dipole) interactions, it is easier to produce stable excited states, with larger values of the added vorticity, in the latter case. Therefore, we here consider long-range dipole-dipole interactions, adopting the scheme introduced in Ref. [37] (the case of contact repulsive interactions, which produces essentially different results, will be considered elsewhere [45]): an effectively two-dimensional BEC composed of atoms carrying electric dipole moments, $g(r)$, which are induced by a polarizing field, $E(r)$, directed perpendicular to the system's (x,y) plane, and with the field's strength growing along the radial coordinate, r:

$$g(r) = \chi E(r), \tag{1}$$

where χ is the atomic polarizability. The spatially modulated field may be imposed by an external capacitor with the separation between its electrodes decreasing with the increase of r [37]. Because two components of the spinor BEC corresponds to different hyperfine states of the same atom, identical dipole moments are induced in both components. In the mean-field approximation, the dynamics of the spinor wave function, $\psi = (\psi_+, \psi_-)$, is governed by the scaled form of the Gross-Pitaevskii equation

$$i\partial_t \psi_\pm = -\frac{1}{2}\nabla^2 \psi_\pm \pm \lambda \hat{D}^{[\mp]}\psi_\mp + g(\mathbf{r})\psi_\pm \times \int d\mathbf{r}' R(\mathbf{r}-\mathbf{r}')g(\mathbf{r}')[|\psi_+(\mathbf{r}')|^2+|\psi_-(\mathbf{r}')|^2], \tag{2}$$

where $\hat{D}^{[\pm]} = \partial_x \pm i\partial_y$ are the SO-coupling operators with strength λ. Because the dipoles are perpendicular to the 2D plane, the kernel of the dipole-dipole interactions is

$$R(\mathbf{r}-\mathbf{r}') = 1/[\epsilon^2 + |(\mathbf{r}-\mathbf{r}')|^2]^{3/2}, \tag{3}$$

where cutoff ϵ is determined by the confinement length $a_\perp$ in the transverse dimension, whose typical size in underlying physical units is

$$a_\perp \sim 3\ \mu\text{m} \tag{4}$$

[46]. As mentioned above, it was demonstrated in Ref. [37] that the spatially modulated repulsive dipole-dipole interactions can create 2D solitons, provided that the magnitude of the locally induced dipole moment grows in r faster than r^3, therefore we here adopt the modulation profile

$$g(r) = \alpha r^4 + g_0, \tag{5}$$

with $\alpha > 0$ and $g_0 \geqslant 0$.

Stationary solutions to Eq. (2) are sought for in the usual form, $\psi_\pm(\mathbf{r},t) = \phi_\pm(\mathbf{r})e^{-i\mu t}$, where $\phi_\pm$ are stationary wave functions and μ is a real chemical potential. The solitons are characterized by the total norm, which is proportional to the number of atoms in the binary BEC

$$N = N_+ + N_- = \int d\mathbf{r}(|\phi_+|^2 + |\phi_-|^2). \tag{6}$$

The system's energy is

$$E = E_{\rm K} + E_{\rm DD} + E_{\rm SO}, \tag{7}$$

where $E_{\rm K}$, $E_{\rm DD}$, and $E_{\rm SO}$ are the kinetic, dipole-dipole, and SO-coupling energies, respectively:

$$\begin{aligned} E_{\rm K} &= \frac{1}{2}\int d\mathbf{r}(|\nabla\phi_+|^2 + |\nabla\phi_-|^2), \\ E_{\rm DD} &= \frac{1}{2}\iint d\mathbf{r}d\mathbf{r}' g(\mathbf{r})[|\phi_+(\mathbf{r})|^2 + |\phi_-(\mathbf{r})|^2] \\ &\quad \times R(\mathbf{r}-\mathbf{r}')g(\mathbf{r}')[|\phi_+(\mathbf{r}')|^2 + |\phi_-(\mathbf{r}')|^2], \\ E_{\rm SO} &= \lambda \int d\mathbf{r}(\phi_+^* \hat{D}^{[+]}\phi_- - \phi_-^* \hat{D}^{[-]}\phi_+). \end{aligned} \tag{8}$$

While all the quantities in Eqs. (2) to (8) are written in the scaled form, as a result units are not necessary in the figures displayed below, it is relevant to summarize here estimates for the relevant quantities in physical units, using, in particular, estimates elaborated in Refs. [34] and [37] for related settings. First, the characteristic values of the atomic or molecular electric polarizability relevant to experiments with ultracold gases may be taken as $\sim 100 \text{Å}^3$, with the corresponding atomic or molecular weight being $M \sim 100$ [47]. The effective scattering length of the dipole-dipole interactions, which is sufficient for the formation of localized modes is

$$a_{\rm DD} \sim 1\ \text{nm} \tag{9}$$

[48]. As it follows from Eqs. (1) to (3), the corresponding intensity of the dipole-dipole interactions is induced by the polarizing dc electric field in a range of ~ 10 kV/cm (which means that voltage ~ 10 V should be applied to the polarizing capacitor with the separation $\sim 10\ \mu$m between its electrodes). The results reported below are relevant to the experimental realization if, in the scaled units adopted here, $x = 1$ corresponds to the physical distance $\sim 10\ \mu$m. This, in turn, implies that the normalization $\lambda = 1$ adopted below in the scaled units represents the physical strength of the SO coupling $\lambda \sim 10^{-6}$ g $\times$ $\mu\text{m}^3/(\text{ms})^2$. More appropriate, in this context, is the estimate for the effective length of the SO coupling,

$$a_{\rm SO} = \hbar^2/(m\lambda) \sim 0.5\ \mu\text{m}, \tag{10}$$

where m is the atomic mass in physical units. This range of values of the SO-coupling strength is accessible to the current experiments [24–26,34]. Finally, it follows from the estimates given by Eqs. (4), (9), and (10) that the values of the scaled norm N in the range of 1–5, which appear in the results reported below, correspond to the number of atoms 10^4–10^5 in the quasi-2D soliton, which should make the observation of the so-predicted self-trapped states definitely possible [49].

II. SEMIVORTICES AND THEIR STABLE EXCITED STATES

The fundamental SVs and excited states generated from them, with chemical potential $\mu < 0$, can be produced by

the following ansatz, written in polar coordinates (r,θ), and adopted as initial conditions for imaginary-time simulations [50,51]

$$\phi_{\pm} = A_{\pm} r^{|S_{\pm}|} \exp(-i\mu t - \alpha_{\pm} r^2 + iS_{\pm}\theta), \tag{11}$$

where $A_{\pm}$ and $\alpha_{\pm}$ are positive constants, and the integer topological-charge numbers $S_{\pm}$ are related by

$$S_- = S_+ + 1 \tag{12}$$

[16]. Fundamental SVs are produced by $(S_+,S_-) = (-1,0)$ or $(0,+1)$, while the excited state of SVs correspond to $(S_+,S_-) = (n,n+1)$, where $n \neq -1$ or 0. In fact, generic solutions in the form of SVs and their excited states exactly agree with a generalized form of the ansatz based on Eqs. (11) and (12) [16]:

$$\begin{aligned} \phi_+ &= r^{|S_+|}\Phi_+(r)\exp(iS_+\theta), \\ \phi_- &= r^{|S_+|+1}\Phi_-(r)\exp[i(S_+ + 1)\theta], \end{aligned} \tag{13}$$

with real functions taking finite values at $r = 0$ and exponentially decaying $\sim \exp(-\sqrt{-\mu}r)$ at $r \to \infty$.

Another type of 2D self-trapped composite state supported by the SO-coupled BEC corresponds to MMs and their excited states, which can be obtained starting from the following ansatz:

$$\begin{aligned} \phi_{\pm} = {} & A_1 r^{|S_1|}\exp(-\alpha_1 r^2 \pm iS_1\theta) \\ & \mp A_2 r^{|S_2|}\exp(-\alpha_2 r^2 \mp iS_2\theta), \end{aligned} \tag{14}$$

where $A_{1,2}$ and $\alpha_{1,2}$ are again positive constants, and the topological-charge numbers are subject to a relation similar to Eq. (12): $S_2 = S_1 + 1$. Actually, ansatz (14) is the superposition of a pair of expressions in the form of ansatz (11) with $S_+ = S_1$ and its mirror image, with $S_+ = -(S_1 + 1)$. On the other hand, unlike the exact ansatz (13) for the SVs, there is no exact generic expression for the MMs. Fundamental MMs correspond to $(S_1,S_2) = (-1,0)$ and $(S_1,S_2) = (0,+1)$, whereas the excited states of MM are generated by the other integer value of (S_1,S_2).

Because the SO coupling naturally creates the orbital angular momentum (OAM) in BEC, we define the normalized OAM of each component, and the total normalized OAM:

$$\langle L_{\pm}\rangle = \frac{\int d\mathbf{r}\phi_{\pm}^{*}\hat{L}\phi_{\pm}}{N_{\pm}}, \quad \langle L\rangle = \frac{N_+\langle L_+\rangle + N_-\langle L_-\rangle}{N}, \tag{15}$$

where $\hat{L} = -i(x\partial_y - y\partial_x)$ is the OAM operator.

Stationary solutions for SVs and their excited states were generated by means of the imaginary-time integration of Eq. (2) (where we adopt the normalization $\lambda = 1$, as said above), initiated by the input given by Eqs. (11) and (12) with integer S_+. Then, the stability of the so-obtained states was tested by means of real-time simulations. This scenario is relevant for making sure that the imaginary-time evolution produced the relevant solutions (for a given norm). Indeed, it may happen, in some cases, that the trajectory of the imaginary-time evolution passes very close to a saddle point, and gets stuck there, which is an obstacle for producing the target states. For this reason, it is commonly adopted to run real-time simulations following the imaginary-time integration (see, e.g., Ref. [52]).

We apply rescaling to fix $\alpha = 1$ in Eq. (5), and, following Ref. [37], we take $g_0 = 0$ and $\epsilon = 0.5$, with other values of these parameters producing quite similar results. The imaginary-time simulations readily produce SVs and their excited states with all integer values of the topological charge, $S_+ = 0, \pm 1, \pm 2, \pm 3, \ldots$. Typical examples of *stable* SVs and their excited states with $S_+ = 0,1,2,3$, and 4 are displayed in Fig. 1(a), the respective total-density pattern $|\psi_+|^2 + |\psi_-|^2$ being a perfect ring, as seen in the third row of Fig. 1(a). Further, families of SVs and their excited states are characterized, as usual, by dependencies $\mu(N)$ and $E(N)$ for them for different values of S_+, which are displayed in Figs. 2(a) and 2(b). They first of these satisfies the *anti-Vakhitov-Kolokolov* criterion, i.e., $d\mu/dN > 0$, which is a known necessary condition of the stability of bright solitons supported by self-repulsive nonlinearities [53,54]. The solitons with topological numbers $(S_+,S_-) = (n,n+1)$ and $(-n-1,-n)$ (where $n \geqslant 0$ is an arbitrary integer) obviously have identical energies and chemical potentials, therefore, we only consider the case of $S_+ \geqslant 0$ for these types of solitons. In the case of $S_+ \geqslant 0$, at $N \to 0$, evident limit values are $\mu \to |S_+| - 0.5$ and $E \to 0$ [16].

The normalized OAM of each component of the SVs and their excited states, defined by Eq. (15), are $\langle L_{\pm}\rangle \equiv S_{\pm}$, i.e., both components of the excited states of SVs are eigenstates of the OAM operator. The component with a smaller value of $|S_{\pm}|$ accounts for a larger contribution to the total norm, in agreement with the trend found for the SVs in Ref. [16]. The total normalized OAM $\langle L\rangle$ is displayed versus N for different values of S_+ in Fig. 2(c), with $\langle L\rangle = S_+ + 0.5$ in the limit of $N \to 0$. At $N > 1$, $\langle L\rangle$, which is slightly smaller than $S_+ + 0.5$, almost does not depend on N. This last result indicates that the SVs and their excited states may be approximately regarded as effectively having a half-integer eigenvalue of the normalized OAM.

As mentioned above, the stability of the SVs and their excited states was verified by means of direct real-time simulations, using the split-step fast-Fourier-transform algorithm. We have thus found that the excited state of SVs are completely stable in this setting for $S_+ \leqslant 5$. A typical example of the stable evolution of the excited state with $S_+ = 5$ is displayed in Fig. 3(a). At $S_+ \geqslant 6$, the excited states of SVs are less stable, with some corrugation appearing in the vortex rings in the course of the long-time propagation. Nevertheless, the excited state of SVs keep their overall vortex structure. A typical example of them with $S_+ \geqslant 6$ is displayed in Fig. 3(b).

The observed stabilization of the vortex solitons with large values of S is a noteworthy finding, as such solitons tend to be unstable in the majority of models of nonlinear media, spontaneously splitting into fragments the number of which being equal or close to $|S|$ [55–58]. Stable vortex solitons with $S > 1$ were found in Bessel lattices with self-defocusing nonlinearity [59], and, more recently, in radial ring-lattices with repulsive dipole-dipole interactions [35], as well as in the other model with the effectively nonlinear interaction, which corresponds to a binary BEC with the components coupled by a microwave field [60] (in the latter case, the components represent two hyperfine atomic states coupled by a magnetic transition). In this connection, it is relevant to mention that

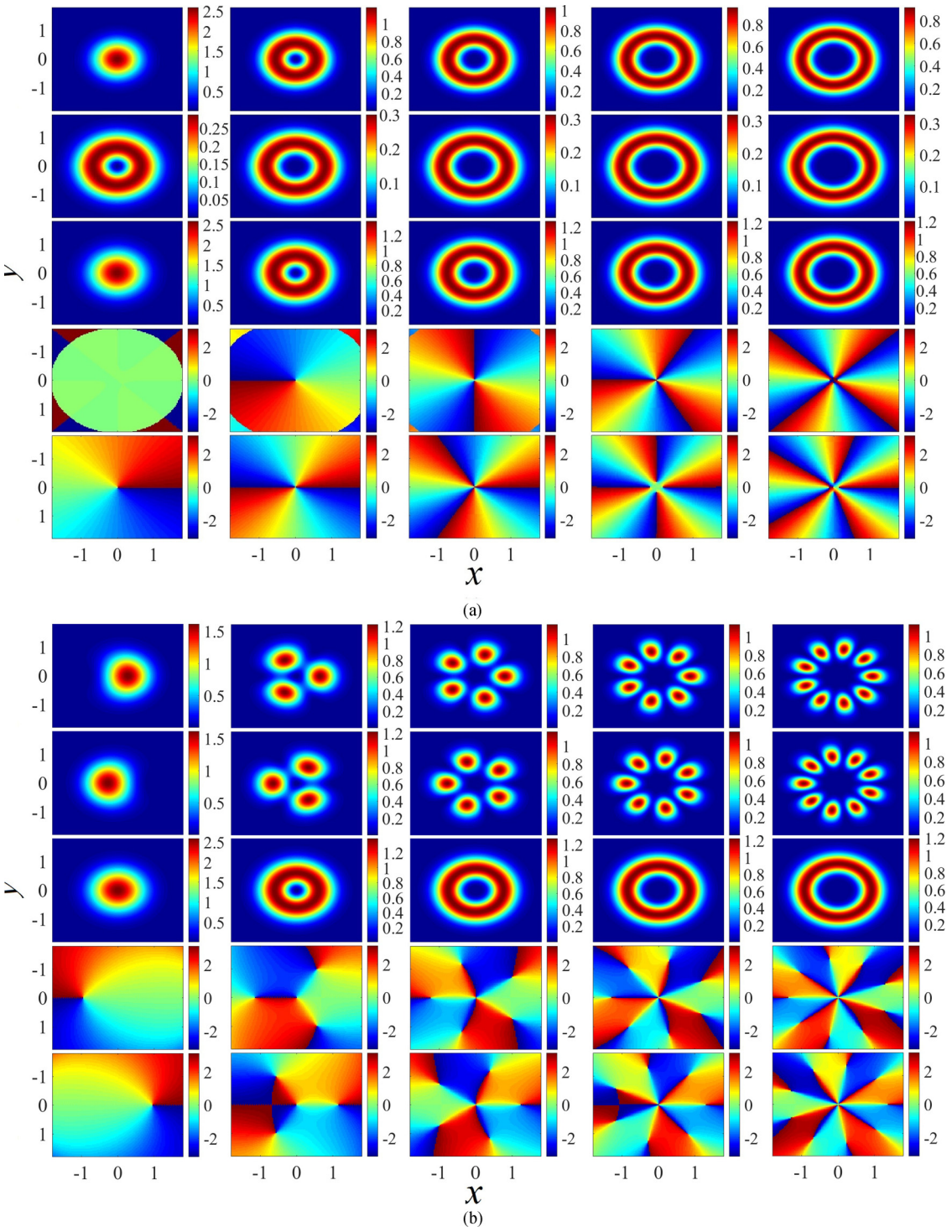

FIG. 1. (a) The first and second rows: density patterns of the ϕ_+ and ϕ_- components of the fundamental SVs and their excited states. The third row: the total-density patterns of the binary BEC, i.e., $|\phi_+|^2 + |\phi_-|^2$. The fourth and fifth rows: phase patterns of ϕ_+ and ϕ_-, respectively. From left to right: $S_+ = 0,1,2,3$, and 4. (b) Similar results for the MMs and their excited states, with the same meaning of the rows as in (a). From left to right: $S_1 = 0$, 1,2,3, and 4. The total norm of all the soliton modes displayed in the figure is $N = 4$.

matter-wave fields carrying definite values of the OAM have various applications to quantum-information processing and optical communications [61–67], hence the stable excited state of SVs with large values of S may help to expand the range of the potential applications [60].

III. MIXED MODES AND THEIR STABLE EXCITED STATES

Stationary solutions for the MMs and their excited states were produced by imaginary-time simulations of Eq. (2) with input (14), setting $S_1 = 0, \pm 1, \pm 2, \ldots$. The solutions produced

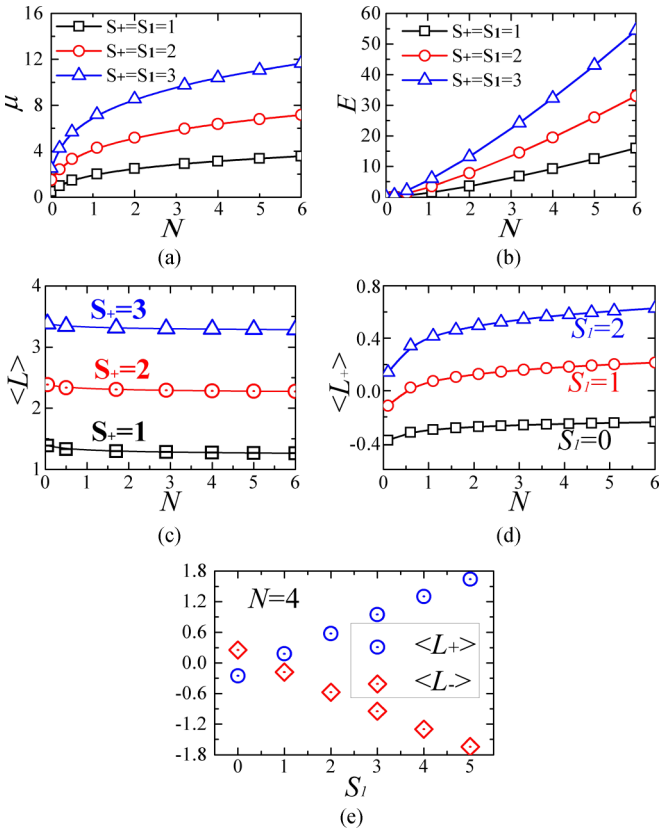

FIG. 2. (a) The chemical potential μ and (b) energy E for *both* excited states of SVs and MM as functions of the total norm N (the coincidence of the curves for the excited states of SVs and MM is explained in the main text). Black curves with squares, red curves with circles, and blue curves with triangles correspond to $S_+ = S_1 = 1$, 2, and 3, respectively. (c) The total normalized orbital angular momentum values $\langle L\rangle$ of excited state of SVs versus N for different values of S_+. (d) The normalized orbital angular momentum for component ϕ_+, i.e., $\langle L_+\rangle$, of excited states of MM versus N for different values of S_1. (e) Values of $\langle L_\pm\rangle$ for excited states of MM versus S_1 for $N = 4$. (Note that $\langle L_-\rangle \equiv -\langle L_+\rangle$ for excited states of MM).

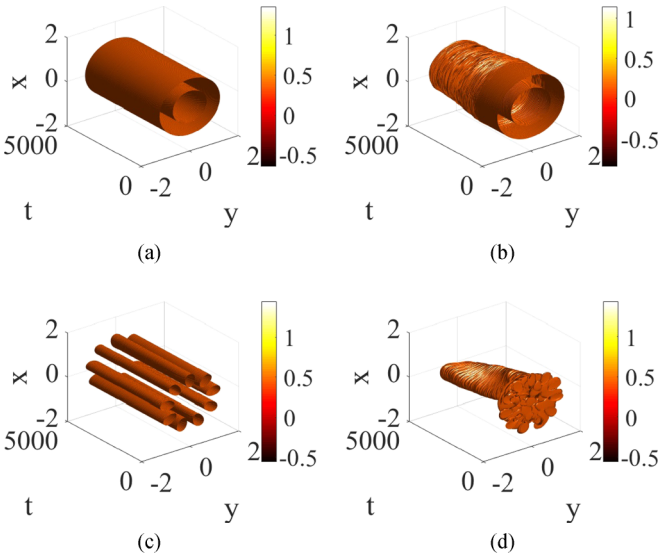

FIG. 3. Long real-time evolution of the density pattern $|\psi_+(t)|^2$, with 3% random noise added to the initial conditions in all panels here. (a) A stable excited state of SVs mode with $(N, S_+) = (4,5)$. (b) An unstable excited state of SVs with $(N, S_+) = (4,6)$. (c) A stable excited state of MM with $(N, S_1) = (4,4)$. (d) An unstable excited state of MM with $(N, S_1) = (4,5)$. All the panels are shown as isosurfaces of $0.4 \times |\psi_+^{\max}(t = 0)|^2$.

by $S_1 = -(n + 1)$ are tantamount to those obtained with $S_1 = n$ ($n \geqslant 0$), therefore, we consider only the case of $S_1 \geqslant 0$ for states of this type. Unlike the SVs and their excited states, the modes of the MMs and their excited states' types naturally have equal norms of the two components, i.e., $N_+ = N_-$. Typical examples of stable MMs and their excited states with $S_1 = 0, 1, 2, 3,$ and 4 are displayed in Fig. 1(b). Numerical results reveal that the established excited states of MM in each component is built as a necklace ring, with the number of fragments exactly equal to $S_1 + S_2 \equiv 2S_1 + 1$.

The results reported in Ref. [16] demonstrated that chemical potentials and energies of the SVs and MMs coincide ($\mu_{\rm SV} = \mu_{\rm MM}$ and $E_{\rm SV} = E_{\rm MM}$) for the systems of the Manakov's type, with equal coefficients of the contact self-attraction and cross-attraction [68]. Because dipole-dipole interactions in Eq. (2) automatically satisfy the Manakov's condition, the excited states of SVs and MM with $S_+ = S_1$ also have equal chemical potentials and energies. Therefore, the plots in Fig. 2(a) and 2(b) represent curves of $\mu(N)$ and $E(N)$, respectively, for excited states of SVs and MM alike, for given values of S_1.

The stability of the excited states was verified through direct real-time simulations. We find that excited states of MM are stable at $S_1 \leqslant 4$ and unstable at $S_1 \geqslant 5$. Typical examples of the evolution of stable and unstable excited states of MM are displayed in Figs. 3(c) and 3(d). In particular, Fig. 3(d) shows that unstable excited states of MM develop spontaneous twist at the initial stage of the evolution, and eventually degenerate into fundamental MMs.

The complexity of the phase patterns of the excited states of MM increases with the increase of the number of fragments in the corresponding necklace, i.e., with the growth of S. The ansatz written in Eq. (14) demonstrates that the MMs and their excited states may be considered as mixtures of two different eigenstates of the OAM operator, therefore the normalized OAM of each component, defined as per Eq. (15), no longer takes integer values, being functions of N and S_1, with the total normalized OAM being zero, $\langle L_+\rangle + \langle L_-\rangle \equiv 0$. Figures 2(d) and 2(e) show $\langle L_+(N)\rangle$ for different values of S_1, and $\langle L_\pm(S_1)\rangle$ for $N = 4$, respectively. These figures demonstrate that $\langle L_+\rangle$ gradually increases with the growth of N and S_1 .

It is interesting to note that spatial positions of fragments ("beads") of the necklace in one component are located exactly in the middle of positions of two adjacent fragments of the other component [see the panels in first and second rows of Fig. 1(b)]. This feature causes the overall density pattern $|\phi_+|^2 + |\phi_-|^2$ to exhibit a profile of a perfect ring. For a given value of total norm N, the total-density patterns of the excited states of SVs and MM are identical for $S_1 = S_+$ [see the third rows in Figs. 1(a) and 1(b)], while, as mentioned above, the total normalized OAM of the excited states of MM vanishes, $\langle L\rangle = (\langle L_+\rangle + \langle L_-\rangle)/2 \equiv 0$, on the contrary to nonzero $\langle L\rangle$ for the excited states of SVs. Moreover, because the normalized OAM for each component is different from zero, $\langle L_+\rangle = -\langle L_-\rangle \neq 0$,

the two-component MMs and their excited states resemble, in terms of photonics, linearly polarized light split into left and right circularly polarized components. In this connection, it is relevant to mention that the splitting of linearly polarized light beams into left- and right-polarized waves finds diverse applications in chiral media and topological photonics [69–74], suggesting that similar applications, such as the realization of topological insulators, may be also realized in terms of the matter waves.

IV. CONCLUSION

The objective of this work was to stabilize the 2D excited states of SVs (semivortices) and MM (mixed mode) in spin-orbit-coupled BECs in the setting based on the dipole-dipole interactions between originally isotropic atoms, induced by a polarizing field oriented perpendicular to the plane in which the BEC is trapped, under the assumption that the strength of the polarizing field grows in the radial direction as r^4. Stable excited states of SVs and MM are predicted in this setting for the first time. They have a size $\sim 10\,\mu$m, and may contain up to 10^5 atoms. Both components of the excited states of SVs are eigenstates of the OAM (orbital angular momentum), the total normalized OAM of such a soliton being $\langle L\rangle \approx S_+ - 0.5$. The characteristics and stability of these excited states of SVs have been systematically studied. They are completely stable at $S_+ \leqslant 5$ and become weakly unstable for $S_+ \geqslant 6$. The excited states of MM feature a circular necklace structure with mutually interleaved components, whose total-density pattern is a perfect ring. The values of the normalized OAM of the two components of the excited states of MM are $\langle L_+\rangle = -\langle L_-\rangle$, with the vanishing total OAM, $\langle L_+\rangle + \langle L_-\rangle \equiv 0$. The excited states of MM are stable at $S_1 \leqslant 4$, and become unstable at $S_1 \geqslant 5$. The characteristics of the stable excited states of SVs and MM suggest that they may find potential applications to high-precision communications, as well as to the design of chiral media and topological insulators for matter waves.

ACKNOWLEDGMENTS

C.H. and Y.L. appreciate the very useful discussions from Prof. Chaohong Lee. This work is supported, in a part, by the National Natural Science Foundation of China (Grants No. 11575063, No. 61705035, No. 11204037, and No. 61575041), and by Grant No. 2015616 from the joint program in physics between the NSF (US) and Binational (US-Israel) Science Foundation, and by Grant No. 1286/17 from the Israel Science Foundation.

[1] B. A. Malomed, D. Mihalache, F. Wise, and L. Torner, Spatiotemporal optical solitons, J. Opt. B: Quantum Semiclassical Opt. **7**, R53 (2005); Viewpoint: On multidimensional solitons and their legacy in contemporary Atomic, Molecular and Optical physics, J. Phys. B: At. Mol. Opt. Phys. **49**, 170502 (2016).

[2] D. Mihalache, Multidimensional localized structures in optics and Bose-Einstein condensates: A selection of recent studies, Rom. J. Phys. **59**, 295 (2014).

[3] M. Segev, G. C. Valley, B. Crosignani, P. DiPorto, and A. Yariv, Steady-State Spatial Screening Solitons in Photorefractive Materials with External Applied Field, Phys. Rev. Lett. **73**, 3211 (1994).

[4] D. Mihalache, D. Mazilu, B. A. Malomed, F. Lederer, L.-C. Crasovan, Y. V. Kartashov, and L. Torner, Stable three-dimensional optical solitons supported by competing quadratic and self-focusing cubic nonlinearities, Phys. Rev. E **74**, 047601 (2006).

[5] D. Mihalache, D. Mazilu, F. Lederer, Y. V. Kartashov, L.-C. Crasovan, L. Torner, and B. A. Malomed, Stable Vortex Tori in the Three-Dimensional Cubic-Quintic Ginzburg-Landau Equation, Phys. Rev. Lett. **97**, 073904 (2006).

[6] D. Mihalache, D. Mazilu, F. Lederer, B. A. Malomed, Y. V. Kartashov, L.-C. Crasovan, and L. Torner, Three-dimensional spatiotemporal optical solitons in nonlocal nonlinear media, Phys. Rev. E **73**, 025601(R) (2006).

[7] S. Skupin, O. Bang, D. Edmundson, and W. Królikowski, Stability of two-dimensional spatial solitons in nonlocal nonlinear media, Phys. Rev. E **73**, 066603 (2006).

[8] C. Rotschild, M. Segev, Z. Xu, Y. V. Kartashov, L. Torner, and O. Cohen, Two-dimensional multipole solitons in nonlocal nonlinear media, Opt. Lett. **31**, 3312 (2006).

[9] P. Pedri and L. Santos, Two-Dimensional Bright Solitons in Dipolar Bose-Einstein Condensates, Phys. Rev. Lett. **95**, 200404 (2005).

[10] R. Nath, P. Pedri, and L. Santos, Stability of Dark Solitons in Three-Dimensional Dipolar Bose-Einstein Condensates, Phys. Rev. Lett. **101**, 210402 (2008).

[11] I. Tikhonenkov, B. A. Malomed, and A. Vardi, Vortex solitons in dipolar Bose-Einstein condensates, Phys. Rev. A **78**, 043614 (2008).

[12] I. Tikhonenkov, B. A. Malomed, and A. Vardi, Anisotropic Solitons in Dipolar Bose-Einstein Condensates, Phys. Rev. Lett. **100**, 090406 (2008).

[13] M. Raghunandan, C. Mishra, K. Lakomy, P. Pedri, L. Santos, and R. Nath, Two-dimensional bright solitons in dipolar Bose Einstein condensates with tilted dipoles, Phys. Rev. A **92**, 013637 (2015); X. Chen, Y. Chuang, C. Lin, C. Wu, Y. Li, B. A. Malomed, and R. Lee, Magic tilt angle for stabilizing two-dimensional solitons by dipole-dipole interactions, *ibid.* **96**, 043631 (2017).

[14] J. Huang, X. Jiang, H. Chen, Z. Fan, W. Pang, and Y. Li, Quadrupolar matter-wave soliton in two-dimensional free space, Front. Phys. **10**, 100507 (2015).

[15] R. M. Wilson, B. M. Anderson, and C. W. Clark, Meron Ground State of Rashba Spin-Orbit-Coupled Dipolar Bosons, Phys. Rev. Lett. **111**, 185303 (2013).

[16] H. Sakaguchi, B. Li, and B. A. Malomed, Creation of two-dimensional composite solitons in spin-orbit-coupled self-attractive Bose-Einstein condensates in free space, Phys. Rev. E **89**, 032920 (2014).

[17] X. Jiang, Z. Fan, Z. Chen, W. Pang, Y. Li, and B. A. Malomed, Two-dimensional solitons in dipolar Bose-Einstein condensates with spin-orbit coupling, Phys. Rev. A **93**, 023633 (2016).

[18] H. Sakaguchi, E. Y. Sherman, and B. A. Malomed, Vortex solitons in two-dimensional spin-orbit coupled Bose-Einstein condensates: Effects of the Rashba-Dresselhaus coupling and Zeeman splitting, Phys. Rev. E **90**, 032202 (2014).

[19] S. Gautam and S. K. Adhikari, Vortex-bright solitons in a spin-orbit-coupled spin-1 condensate, Phys. Rev. A **95**, 013608 (2017).

[20] G. Chen, Y. Liu, and H. Wang, Mixed-mode solitons in quadrupolar BECs with spin-orbit coupling, Commun. Nonlinear Sci. Numer. Simulat. **48**, 318 (2017).

[21] Y. Zhang, Z. Zhou, B. A. Malomed, and H. Pu, Stable Solitons in Three-Dimensional Free Space without the Ground State: Self-Trapped Bose-Einstein Condensates with Spin-Orbit Coupling, Phys. Rev. Lett. **115**, 253902 (2015).

[22] Y. Li, Z. Luo, Y. Liu, Z. Chen, C. Huang, S. Fu, H. Tan, and B. A. Malomed, Two-dimensional solitons and quantum droplets supported by competing self- and cross-interactions in spin-orbit-coupled condensates, New J. Phys. **19**, 113043 (2017).

[23] B. Liao, S. Li, C. Huang, Z. Luo, W. Pang, H. Tan, B. A. Malomed, and Y. Li, Anisotropic semi-vortices in dipolar spinor condensates controlled by Zeeman splitting, Phys. Rev. A **96**, 043613 (2017).

[24] Y. J. Lin, K. Jimenez-Garcia, and I. B. Spielman, Spin-orbit-coupled Bose-Einstein condensates, Nature (London) **471**, 83 (2011).

[25] H. Zhai, Degenerate quantum gases with spin-orbit coupling: A review, Rep. Prog. Phys. **78**, 026001 (2015).

[26] Y. Zhang, M. E. Mossman, T. Busch, P. Engels, and C. Zhang, Properties of spin-orbit-coupled Bose-Einstein condensates, Front. Phys. **11**, 118103 (2016).

[27] H. Sakaguchi and B. A. Malomed, One- and two-dimensional solitons in $\mathcal{PT}$-symmetric systems emulating the spin-orbit coupling, New J. Phys. **18**, 105005 (2016).

[28] Y. V. Kartashov, V. V. Konotop, and F. Kh. Abdullaev, Gap Solitons in a Spin-Orbit-Coupled Bose-Einstein Condensate, Phys. Rev. Lett. **111**, 060402 (2013).

[29] Y. V. Kartashov and V. V. Konotop, Solitons in Bose-Einstein Condensates with Helicoidal Spin-Orbit Coupling, Phys. Rev. Lett. **118**, 190401 (2017).

[30] V. E. Lobanov, Y. V. Kartashov, and V. V. Konotop, Fundamental, Multipole, and Half-Vortex Gap Solitons in Spin-Orbit Coupled Bose-Einstein Condensates, Phys. Rev. Lett. **112**, 180403 (2014).

[31] Y. Xu, Y. Zhang, and C. Zhang, Bright solitons in a 2D spin-orbit-coupled dipolar Bose-Einstein condensate, Phys. Rev. A **92**, 013633 (2015).

[32] Y. Xu, Y. Zhang, and B. Wu, Bright solitons in spin-orbit-coupled Bose-Einstein condensates, Phys. Rev. A **87**, 013614 (2013).

[33] L. Salasnich, W. B. Cardoso, and B. A. Malomed, Localized modes in quasi-two-dimensional Bose-Einstein condensates with spin-orbit and Rabi couplings, Phys. Rev. A **90**, 033629 (2014).

[34] B. Ramachandhran, B. Opanchuk, X.-J. Liu, H. Pu, P. D. Drummond, and H. Hu, Half-quantum vortex state in a spin-orbit-coupled Bose-Einstein condensate, Phys. Rev. A **85**, 023606 (2012).

[35] C. Huang, L. Lyu, H. Huang, Z. Chen, S. Fu, H. Tan, B. A. Malomed, and Y. Li, Dipolar bright solitons and solitary vortices in a radial lattice, Phys. Rev. A **96**, 053617 (2017).

[36] Y. Li, Y. Liu, Z. Fan, W. Pang, S. Fu, and B. A. Malomed, Two-dimensional dipolar gap solitons in free space with spin-orbit coupling, Phys. Rev. A **95**, 063613 (2017).

[37] Y. Li, J. Liu, W. Pang, and B. A. Malomed, Matter-wave solitons supported by field-induced dipole-dipole repulsion with spatially modulated strength, Phys. Rev. A **88**, 053630 (2013).

[38] F. Kh. Abdullaev, A. Gammal, B. A. Malomed, and L. Tomio, Bright solitons in Bose-Einstein condensates with field-induced dipole moments, J. Phys. B **47**, 075301 (2014).

[39] O. V. Borovkova, Y. V. Kartashov, B. A. Malomed, and L. Torner, Algebraic bright and vortex solitons in defocusing media, Opt. Lett. **36**, 3088 (2011).

[40] O. V. Borovkova, Y. V. Kartashov, L. Torner, and B. A. Malomed, Bright solitons from defocusing nonlinearities, Phys. Rev. E **84**, 035602 (2011).

[41] Q. Tian, L. Wu, Y. Zhang, and J.-F. Zhang, Vortex solitons in defocusing media with spatially inhomogeneous nonlinearity, Phys. Rev. E **85**, 056603 (2012).

[42] Y. Wu, Q. Xie, H. Zhong, L. Wen, and W. Hai, Algebraic bright and vortex solitons in self-defocusing media with spatially inhomogeneous nonlinearity, Phys. Rev. A **87**, 055801 (2013).

[43] R. Driben, Y. V. Kartashov, B. A. Malomed, T. Meier, and L. Torner, Soliton Gyroscopes in Media with Spatially Growing Repulsive Nonlinearity, Phys. Rev. Lett. **112**, 020404 (2014).

[44] Y. V. Kartashov, B. A. Malomed, Y. Shnir, and L. Torner, Twisted Toroidal Vortex-Solitons in Inhomogeneous Media with Repulsive Nonlinearity, Phys. Rev. Lett. **113**, 264101 (2014).

[45] R. Zhong, Z. Chen, C. Huang, Z. Luo, H. Tan, B. A. Malomed, and Y. Li, Self-trapping under the two-dimensional spin-orbit-coupling and spatially growing repulsive nonlinearity, arXiv:1712.01430.

[46] H. T. C. Stoof, K. B. Gubbels, and D. B. M. Dickersheid, *Ultracold Quantum Fields* (Springer, Dordrecht, The Netherlands, 2009).

[47] B. Arora, M. S. Safronova, and C. W. Clark, Determination of electric-dipole matrix elements in K and Rb from Stark shift measurements, Phys. Rev. A **76**, 052516 (2007); S. Ospelkaus, K.-K. Ni, M. H. G. de Miranda, B. Neyenhuis, D. Wang, S. Kotochigova, P. S. Julienne, D. S. Jin, and J. Ye, Ultracold polar molecules near quantum degeneracy, Faraday Discuss. **142**, 351 (2009).

[48] S. Giovanazzi, A. Görlitz, and T. Pfau, Tuning the Dipolar Interaction in Quantum Gases, Phys. Rev. Lett. **89**, 130401 (2002).

[49] K. E. Strecker, G. B. Partridge, A. G. Truscott, and R. G. Hulet, Bright matter wave solitons in Bose-Einstein condensates, New J. Phys. **5**, 73 (2003).

[50] L. M. Chiofalo, S. Succi, and P. M. Tosi, Ground state of trapped interacting Bose-Einstein condensates by an explicit imaginary time algorithm, Phys. Rev. E **62**, 7438 (2000).

[51] J. Yang and T. I. Lakoba, Accelerated imaginary-time evolution methods for the computation of solitary waves, Stud. Appl. Math. **120**, 265 (2008).

[52] R. K. Kumar, T. Sriraman, H. Fabrelli, P. Muruganandam, and A. Gammal, Three-dimensional vortex structures in a rotating dipolar Bose-Einstein condensate, J. Phys. B: At. Mol. Opt. Phys. **49**, 155301 (2016).

[53] N. G. Vakhitov and A. A. Kolokolov, Stationary solutions of the wave equation in a medium with nonlinearity saturation, Radiophys. Quantum Electron. **16**, 783 (1973).

[54] H. Sakaguchi and B. A. Malomed, Solitons in combined linear and nonlinear lattice potentials, Phys. Rev. A **81**, 013624 (2010).

[55] J. M. Soto-Crespo, D. R. Heatley, E. M. Wright, and N. N. Akhmediev, Stability of the higher-bound states in a saturable self-focusing medium, Phys. Rev. A **44**, 636 (1991).

[56] D. V. Skryabin and W. J. Firth, Dynamics of self-trapped beams with phase dislocation in saturable Kerr and quadratic nonlinear media, Phys. Rev. E **58**, 3916 (1998).

[57] M. Soljačić, S. Sears, and M. Segev, Self-Trapping of Necklace Beams in Self-Focusing Kerr Media, Phys. Rev. Lett. **81**, 4851 (1998).

[58] A. S. Desyatnikov and Y. S. Kivshar, Necklace-Ring Vector Solitons, Phys. Rev. Lett. **87**, 033901 (2001).

[59] Y. V. Kartashov, V. A. Vysloukh, and L. Torner, Stable Ring-Profile Vortex Solitons in Bessel Optical Lattices, Phys. Rev. Lett. **94**, 043902 (2005).

[60] J. Qin, G. Dong, and B. A. Malomed, Stable giant vortex annuli in microwave-coupled atomic condensates, Phys. Rev. A **94**, 053611 (2016).

[61] L. Allen, M. W. Beijersbergen, R. J. C. Spreeuw, and J. P. Woerdman, Orbital angular momentum of light and the transformation of Laguerre-Gaussian laser modes, Phys. Rev. A **45**, 8185 (1992).

[62] S. Franke-Arnold, L. Allen, and M. Padgett, Advances in optical angular momentum, Laser Photonics Rev. **2**, 299 (2008).

[63] X. Cai, J. Wang, M. J. Strain, B. Johnson-Morris, J. Zhu, M. Sorel, J. L. O'Brien, M. G. Thompson, and S. Yu, Integrated compact optical vortex beam emitters, Science **338**, 363 (2012).

[64] J. Wang, J. Yang, I. M. Fazal, N. Ahmed, Y. Yan, H. Huang, Y. Ren, Y. Yue, S. Dolinar, M. Tur, and A. E. Willner, Terabit free-space data transmission employing orbital angular momentum multiplexing, Nat. Photonics **6**, 488 (2012).

[65] M. J. Padgett, F. M. Miatto, M. P. J. Lavery, A. Zeilinger, and R. W. Boyd, Divergence of an orbital-angular-momentum-carrying beam upon propagation, New J. Phys. **17**, 023011 (2015).

[66] D. Ding, W. Zhang, Z. Zhou, S. Shi, G. Xiang, X. Wang, Y. Jiang, B. Shi, and G. Guo, Quantum Storage of Orbital Angular Momentum Entanglement in an Atomic Ensemble, Phys. Rev. Lett. **114**, 050502 (2015).

[67] P. Miao, Z. Zhang, J. Sun, W. Walasik, S. Longhi, N. M. Litchinitser, and L. Feng, Orbital angular momentum microlaser, Science **353**, 464 (2016).

[68] D. J. Kaup and B. A. Malomed, Soliton trapping and Daughter Waves in the Manakov model, Phys. Rev. A **48**, 599 (1993).

[69] J. W. Mciver, D. Hsieh, H. Steinberg, P. Jarillo-Herrero, and N. Gedik, Control over topological insulator photocurrents with light polarization, Nat. Nanotechnol. **7**, 96 (2012).

[70] Y. H. Wang, H. Steinberg, P. Jarillo-Herrero, and N. Gedik, Observation of Floquet-Bloch states on the surface of a topological insulator, Science **342**, 453 (2013).

[71] K. Y. Bliokh, F. J. Rodríguez-Fortuño, F. Nori, and A. V. Zayats, Spin-orbit interactions of light, Nat. Photonics **9**, 796 (2015).

[72] Q. Guo, W. Gao, J. Chen, Y. Liu, and S. Zhang, Line Degeneracy and Strong Spin-Orbit Coupling of Light with Bulk Bianisotropic Metamaterials, Phys. Rev. Lett. **115**, 067402 (2015).

[73] M. Rafayelyan, G. Tkachenko, and E. Brasselet, Reflective Spin-Orbit Geometric Phase from Chiral Anisotropic Optical Media, Phys. Rev. Lett. **116**, 253902 (2016).

[74] P. Lodahl, S. Mahmoodian, S. Stobbe, A. Rauschenbeutel, P. Schneeweiss, J. Volz, H. Pichler, and P. Zoller, Chiral quantum optics, Nature **541**, 473 (2017).